INTRACLUSTER COMPTONIZATION OF THE CMB: MEAN SPECTRAL DISTORTION AND CLUSTER NUMBER COUNTS

S. COLAFRANCESCO

Osservatorio Astronomico di Roma
via dell'Osservatorio, I-00040 Monteporzio, Italy

P. MAZZOTTA

Dipartimento di Fisica, Università di Roma "Tor Vergata"
via della Ricerca Scientifica 1, I-00133 Roma, Italy

Y. REPHAELI*

Center for Particle Astrophysics
University of California, Berkeley, CA 94720

Physics Department
Stanford University, Stanford, CA 94305

and

N. VITTORIO

Dipartimento di Fisica, Università di Roma "Tor Vergata"
via della Ricerca Scientifica 1, I-00133 Roma, Italy

Subject headings: cosmic microwave background – cosmology: theory – clusters of galaxies: evolution.

*On leave from School of Physics and Astronomy, Tel Aviv University, Tel Aviv, Israel

Abstract

The mean sky-averaged Comptonization parameter, $\overline{y}$, describing the scattering of the CMB by hot gas in clusters of galaxies is calculated in an array of flat and open cosmological and dark matter models. The models are globally normalized to fit cluster X-ray data, and intracluster gas is assumed to have evolved in a manner consistent with current observations. We predict values of $\overline{y}$ lower than the COBE/FIRAS upper limit. The corresponding values of the overall optical thickness to Compton scattering are $\lesssim 10^{-4}$ for relevant parameter values. Of more practical importance are number counts of clusters across which a net flux (with respect to the CMB) higher than some limiting value can be detected. Such number counts are specifically predicted for the COBRAS/SAMBA and BOOMERANG missions.

1 Introduction

Compton scattering of the cosmic microwave background (CMB) radiation by hot gas in clusters of galaxies – the Sunyaev-Zeldovich (1970; hereafter S-Z) effect – affects both the spectrum and the angular distribution of the radiation. The spectral change of the CMB across each cluster translates into a superposed average change of the spectrum across the sky. When the intensity (or temperature) is differentially measured, the radiation will appear anisotropic, on characteristic angular scales of several arcminutes, reflecting the typical sizes of clusters that contribute most to the anisotropy. This cluster-induced anisotropy is an important component of the full anisotropy on such scales, as has been shown in many studies (see, *e.g.* , Rephaeli 1995a, and references therein).

Less studied is the overall spectral effect of clusters on the CMB. Whereas the anisotropy is a measure of the rms value of the Comptonization parameter y [defined in Equation (12) below], the overall spectral effect results from the superposed effects of individual clusters over the sky. This parameter is of prime interest in the characterization of spectral deviations from a pure blackbody spectrum. Currently, the COBE/FIRAS database provides the best measure of such non-Planckian distortions by constraining the degree of Comptonization to be $y \leq 1.5 \times 10^{-5}$ at

the 90% statistical significance level (Fixsen *et al.* 1996). The significance of this value stems from the fact that it limits the cumulative effects of energy release processes in the early universe (at $z \lesssim 3 \times 10^6$), and the superposed effects of hot intergalactic (IG) and intracluster (IC) gas (Wright *et al.* 1994). In order to predict the contribution to the Comptonization parameter due to a population of evolving clusters, some assumptions need to be made about the evolution of groups and clusters (which, for brevity, will hitherto be collectively referred to as clusters) of galaxies, and basic characteristics of their hot gas. Under these assumptions the distribution of the Comptonization parameter in clusters at different redshifts and in a given mass range can be calculated. From this, the mean Comptonization due to clusters can be reasonably well estimated.

Here we present the results of an investigation of the effects on the CMB of a population of evolving clusters, described in the background of various flat and open cosmological models. In a previous paper (Colafrancesco *et al.* 1994) we have reported results of a calculation of the predicted rms fluctuations in the CMB induced by gas in clusters in a set of flat cosmological models. Because our basic approach here is similar to that detailed in the latter paper, our discussion – in §2 – of the general background and modeling of clusters and of their IC gas will be brief. The basic definitions of the sky-averaged quantities we calculate here are given in §3. We also calculate the expected cluster number counts in the mm and sub-mm bands.

Long duration balloon flights and space missions dedicated to the study of CMB anisotropy are expected to reach sensitivity levels of ≈ 10 μK per pixel. The COBRAS/SAMBA mission (hereafter C/S; see *e.g.* Mandolesi *et al.* 1995), has been selected as the next Medium-Sized Mission of the ESA Horizon 2000 Program. The eight channels of this experiment cover a wide frequency range, from 35 to 714 GHz. In particular, the 140, 222 and 400 GHz channels of the High Frequency Instrument (HFI) are particularly relevant for measurement of the S-Z effect in clusters. The first frequency is on the Rayleigh-Jeans (R-J) side, where the intensity

change (across a cluster) is negative; the second is near the crossover frequency (where the thermal effect vanishes), and the third is on the Wien side, where the effect is positive (for a discussion of the significance of high-frequency measurements, see Rephaeli, 1995a). The corresponding angular resolutions at these frequencies are $10.5'$, $7.5'$, $4.5'$(FWHM), respectively. A long duration balloon-borne experiment BOOMERANG (see Lange *et al.* 1995) is expected to cover a $10^o \times 10^o$ patch of the sky with a FWHM resolution of $5'$at 150 GHz. The projected sensitivity levels and angular resolution of these experiments are very suitable for a survey of a large number of clusters. In §4 we present the results of our calculations giving the predicted ranges of values of basic quantities which can be determined in light of these observational capabilities. Finally, in §5 we assess these results and summarize our main conclusions.

2 Cosmological Evolution of Clusters

2.1 Mass and Redshift Distribution of Clusters

We adopt the simple spherical collapse picture for cluster formation, according to which a homogeneous, spherical perturbation detaches from the Hubble flow at time t_m, collapses at time $t_c \simeq 2t_m$, and virializes at time $t_v \simeq 3t_m$. The relative density contrast at an initial redshift z_i, $\delta_{i,v}$, depends on the cosmological model. Under the assumption of linear growth, the density contrast at t_v is $\delta_v = \delta_{i,v} D(t_v)/D(t_i)$, where $D(t_v)$ is the linear growth factor in the chosen cosmology. The relevant formulae for low density (open, or vacuum dominated) models are given in the Appendix. For $\Omega_0 \to 1$, δ_v tends to the standard value of 2.2, independent of t_v. The actual, non-linear density contrast is $\Delta = \tilde{\rho}/\rho$, where $\tilde{\rho}$ is the perturbation density and ρ is the background density at the time of virialization. In the Appendix we also briefly review how to derive Δ in low density cosmological models. For $z_v \to \infty$, Δ, evaluate at z_v tends to the standard value ≈ 400, found in a flat universe.

The mass and redshift distribution of clusters, $N(M,z)$, can be determined from the Press & Schechter (1974; hereafter P&S) theory:

$$N(M,z) = \frac{\rho}{M}\frac{\delta_v}{\sigma^2}\frac{d\sigma}{dM}\frac{1}{\sqrt{2\pi}}\exp[-\delta_v^2/2\sigma^2]\,, \tag{1}$$

where ρ is the background density at redshift z, M is the total cluster mass, $\sigma(M,z)$ is the *rms* of the linear density fluctuation field at z, smoothed over the region containing M, and δ_v is the linear density contrast of a perturbation that virializes at z. The variance of density fluctuations of mass M is given in the standard relation:

$$\sigma^2(R,z) = D^2(z)\int dlnk\ k^3P(k)\Big[\frac{3j_1(kR)}{kR}\Big]^2 \tag{2}$$

with $M = 4\pi\rho R^3/3$. We use the fitting formulae for the power spectra, $P(k)$, given in Holtzman (1989) in order to calculate the mass variance in different cosmological models. Here we consider flat cold (CDM) and mixed (MDM) dark matter models, low density CDM models with a cosmological constant (CDM+Λ), as well as open, pure baryonic models with isocurvature initial conditions (BDM).

If the power spectrum of density fluctuations is a power-law of the spatial frequency [*i.e.* $P(k) = Ak^n$], then $\sigma(M,z) = (1/b)(M/M_0)^{-\alpha}D(z)$, where M_0 is the mass contained in a sphere of $8h^{-1}Mpc$ radius, b is the biasing factor, and $\alpha = (n+3)/6$. For this power-law spectrum, the mass distribution assumes the well known form:

$$N(M,z) = \frac{\mathcal{I}}{\sqrt{2\pi}}\frac{\rho}{M_0^2}\frac{n+3}{6}\frac{\delta_v b}{D(z)}\Big(\frac{M}{M_0}\Big)^{\alpha-2}\exp\Big[-\frac{1}{2}\frac{\delta_v^2 b^2}{D^2(z)}\Big(\frac{M}{M_0}\Big)^{2\alpha}\Big]\,, \tag{3}$$

where $1 \le \mathcal{I} \le 2$ takes into account possible secondary infall of mass into the cluster after its initial collapse and virialization.

The fact that $N(M,z)$ depends on the product $\delta_v b$, and not separately on δ_v and b, somewhat simplifies the fit to X-ray data. We have determined the values of $\mathcal{I}$ and $\delta_v b$ in various dark matter models by fitting to the observed cluster X-ray luminosity function of Kowalski *et al.*

(1984). The results of our analysis (see Colafrancesco & Vittorio 1994 for details) are showns in Table 1. Using a P&S theory where $\mathcal{I}$ and $\delta_v b$ are fitted to the X-ray luminosity (or temperature) functions, weakens the predictive power of the theoretical models based on the linear theory. However, the fitted values of $\mathcal{I}$ and $\delta_v b$ should contain the relevant informations of a more realistic cluster formation picture.

2.2 Properties and Evolution of Intracluster Gas

There are various open issues pertaining to the formation of the hot gaseous cores of clusters. For our purposes here we can adopt the following simplified approach: shortly after a cluster forms and virializes, a gaseous core forms (probably as a result of tidal galactic interactions and other gas stripping processes) with the hot gas in hydrostatic equilibrium in the potential well of the cluster. To avoid introducing a large number of free parameters, we will simply scale the gas properties to those of the cluster. This is suggested by X-ray observations of local clusters (see, *e.g.* , Jones & Forman 1992). The gas mass is taken to be a fraction f of the total cluster mass, and the gas density profile is assumed to have the commonly adopted form

$$n(r) = n_0[1 + (r/r_c)^2]^{-3\beta/2}\,, \tag{4}$$

where n_0 is the central electron density and r_c is a core radius. The observed values of β range roughly from 0.5 to 0.7. Here we use the value $\beta = 2/3$ which is particularly convenient in analytic calculations.

The radial extent of a cluster is taken as $R = pr_c$. The mass within the outer radius $R(p)$ is

$$M(p) = 3M_0[p - tg^{-1}p]\,, \tag{5}$$

where $M_0 = (4\pi/3)r_c^3\rho_0$, and ρ_0 is the central total mass density of the cluster.

Assuming that cluster collapse is self-similar, we can infer the mass and redshift dependence

of r_c from the scaling law: $r_c = \Big[3M/4\pi\rho_b\Delta\Big]^{1/3}(1+z)^{-1}$. This gives

$$r_c(\Omega_0, M, z) = \frac{1.29\ h^{-1}\ \mathrm{Mpc}}{p}\Big[\frac{M}{10^{15}\,\mathrm{h}^{-1}\ \mathrm{M}_\odot}\cdot\frac{\Delta(\Omega_0=1,z=0)}{\Omega_0\Delta(\Omega_0,z)}\Big]^{1/3}\frac{1}{1+z}\,. \tag{6}$$

Hereafter we fix $p = 10$ to recover values of the IC gas core radii consistent with observations (see, *e.g.* , Sarazin 1988, Jones & Forman 1991). In particular, for a local cluster of $10^{15}\,\mathrm{h}^{-1}\ \mathrm{M}_\odot$ we get $r_c = 0.12$ and $0.16\ h^{-1}$ Mpc for $\Omega_0 = 1$ and $\Omega_0 = 0.2$, respectively.

The gas is assumed isothermal at the virial temperature $T \propto M/R$. This gives

$$T = 8.7\cdot 10^7(1+z)(\frac{M}{10^{15}h^{-1}M_\odot})^{2/3}\cdot\Big[\frac{\Omega_0\Delta(\Omega_0,z)}{\Delta(\Omega_0=1,z=0)}\Big]^{1/3}K. \tag{7}$$

Although it is known that the gas mass fraction depends on z and M, little is currently known on the exact form of these dependences. We adopt the simple parametrization (described in detail in Colafrancesco & Vittorio 1994; see also Cavaliere, Colafrancesco and Menci 1993) which is based on the results of analyses of the *Einstein* Medium Sensitivity Survey (EMSS) data (Gioia *et al.* 1990; Henry *et al.* 1992) which seem to indicate a decrease in the number of bright clusters with redshift, and an analysis of a local cluster sample (David *et al.* 1990):

$$f = f_o\Big(\frac{M}{10^{15}\,\mathrm{h}^{-1}\ \mathrm{M}_\odot}\Big)^{\eta}\Big(\frac{t}{t_o}\Big)^{\xi}. \tag{8}$$

Here t_o is the age of the universe, and the normalization to $f_o \simeq 0.1$, is based on a local, rich cluster sample. Values of η and ξ are listed in Table 1.

3 Cluster Comptonization

In the non-relativistic limit, the effect of scattering of the CMB by hot gas depends linearly on the cluster Comptonization parameter:

$$y_c = \frac{kT}{m_e c^2}\sigma_T\int_{\ell_{min}}^{\ell_{max}} n\,d\ell\,, \tag{9}$$

where σ_T is the Thomson cross section, and the integral is over a line of sight through the cluster. In the exact relativistic treatment, the dependence of the effect is not exactly linear in y. For low values of the optical thickness τ to Compton scattering, the dependence on τ is linear, but the dependence on T is more complicated, even for the observed range of IC gas temperatures, roughly $3 \div 15$ keV. The higher the gas temperature and the observing frequency, the larger is the deviation of the intensity change from the non-relativistic value (Rephaeli 1995b). This must be taken into account in the analysis of high frequency observations of individual rich clusters (Rephaeli 1995a, Holzapfel *et al.* 1996). Here we are interested in the integrated effect due to many clusters, and since we expect this to be largely dominated by the numerous low richness (and, correspondingly, low temperature) clusters (Colafrancesco *et al.* 1994), we retain here the considerable degree of simplicity which results from expressing the full spatial dependence linearly in the Comptonization parameter. The overall effect of this simplification on our results is assessed in the Discussion.

The cumulative Comptonization parameter $y(\hat{\gamma})$ along the line of sight (los) $\hat{\gamma}$ is the sum over all clusters whose gaseous spheres are intersected by this los. Identifying a cluster in the ensemble by its mass M_m and redshift z_l, the expression for $y(\hat{\gamma})$ can be written as (Cole and Kaiser 1988):

$$y(\hat{\gamma}) = \sum_{l,m} n_{l,m} y_o(M_m, z_l) \zeta(|\hat{\gamma} - \hat{\gamma}_l|, M_m, z_l)\,. \tag{10}$$

Here $n_{l,m}$ is the occupation number of clusters in the $M - z$ space, while

$$y_o(M_m, z_l) \equiv (2tg^{-1}p)(kT/m_e c^2)\sigma_T n_o r_c. \tag{11}$$

is the value of the Comptonization parameter along a los, $\hat{\gamma}_l$, through the center of the cluster (with mass M_m at redshift z_l). The angular profile ζ, obtained by integrating the truncated profile of Equation (6) along different directions is

$$\zeta(|\hat{\gamma} - \hat{\gamma}_l|, M, z) = tg^{-1}\Big[p\sqrt{\frac{1-(\theta/p\theta_c)^2}{1+(\theta/\theta_c)^2}}\Big] \Big/ \Big[(tg^{-1}p)\cdot\sqrt{1+(\theta/\theta_c)^2}\Big] \tag{12}$$

where $\cos(\theta) = \hat{\gamma} \cdot \hat{\gamma}_l$, $\theta \leq p\theta_c$, and $\theta_c = \theta_c(M, z)$ is the angle subtended by r_c.

The distribution of IC gas has characteristic angular scales reflecting the apparent sizes of clusters at various redshifts (unlike the case of a possible uniform intergalactic medium). Nevertheless, even though the distribution of values of the Comptonization parameter depends on the beam size, its true sky-averaged value is beam-independent. To find the mean value of the Comptonization parameter, we average $y(\hat{\gamma})$ first over the sky and then over the ensemble of cluster distributions. The sky and the ensemble average act on the profile and the phase space density respectively, yielding

$$\overline{\zeta(M,z)} = \frac{\theta_c^2}{2tg^{-1}p}(p - tg^{-1}p). \tag{13}$$

Altogether, the mean Comptonization parameter averaged over the ensemble of clusters and over the sky is

$$\overline{y} = \int \frac{dV}{dz} dz \int N(M,z) y_o(M,z) \overline{\zeta(M,z)} dM\,. \tag{14}$$

In Table 2 we list values of $\overline{y}$, in the selected open and flat models with the parameters of Table 1 and $M_{min} = 10^{13}\,\mathrm{M}_\odot$. The values of $\overline{y}$ are generally well below the FIRAS upper limit, 1.5×10^{-5} (Fixsen *et al.* 1996).

Because values of most of the parameters are poorly known, it is important to consider the full parameter range. In Table 2 we also list predicted values of $\overline{y}$ obtained with no gas evolution (*i.e.* $\eta = 0$, $\xi = 0$), and with different choices for M_{min}. Based on these estimates we conclude that the assumed degree of IC gas evolution reduces $\overline{y}$ by a factor of few, except in the BDM models where this factor can be very significant. The decrease in the degree of Comptonization with increasing M_{min} is dramatic only in the BDM $\Omega_0 = 0.1$ model. The predicted value of $\overline{y}$ in the BDM $\Omega_0 = 0.1$ model with no gas evolution is inconsistent with the current FIRAS limit, even if M_{min} is increased by a factor of ~ 3 to $M_{min} = 10^{13}\,\mathrm{M}_\odot$.

As shown in Figure 1, most of the contribution to the mean Comptonization comes from clusters at $z \lesssim 2$, if there is gas evolution. For open CDM models without gas evolution there is a substantial contribution to $\overline{y}$ up to $z \lesssim 5$.

Another useful quantity which can be readily calculated using the above formalism is the mean optical thickness to Compton scattering due to gas in clusters. Since the optical thickness of a cluster is $\tau = y \cdot m_e c^2/kT$, the above expressions can be used to calculate $\overline{\tau}$ by simply replacing $y_o(M,z)$ in Equation (15) with $\tau_o(M,z) \equiv y_o(M,z) m_e c^2/kT$, the optical thickness along a los through the center of a cluster of mass M at redshift z. Values of the mean sky-averaged optical thickness of gas in clusters are listed in Table 2. These give a measure of the minimal degree of scattering of the radiation from distant sources. The sensitivity to M_{min} is larger in this case: nonetheless, values $\lesssim 10^{-4}$ are obtained for most of the models. Only in the BDM models with $n = -1$ and without gas evolution does τ attain values of $\gtrsim 10^{-3}$.

4 Cluster Counts

With respect to the incident radiation field, the change of the CMB intensity across a cluster can be viewed as a net flux emanating from the cluster. The flux is negative below the crossover frequency and positive above this characteristic frequency ($\simeq 217$ GHz in the nonrelativistic limit). While the main emphasis so far has been the measurement of the S-Z effect in individual clusters, the capability to observe a large number of clusters in a satellite survey enhances interest in S-Z number counts. The number of clusters observable in sub-mm bands is of particular interest in view of forthcoming experiments dedicated to the study of the small scale structure of CMB anisotropy. In the nonrelativistic limit, the change of spectral intensity across a cluster of a given y, observed at a frequency $x = h\nu/kT_{CMB}$ [$T_{CMB} = (2.726 \pm 0.010)$ K; Mather *et al.* 1994), is

$$\Delta I_\nu = \frac{2(kT_{CMB})^3}{(hc)^2} g(x) y \,, \tag{15}$$

where

$$g(x) = \frac{x^4 e^x}{(e^x - 1)^2} \cdot [x coth(x/2) - 4] \,. \tag{16}$$

The differential flux measured at a given frequency from the cluster is

$$\Delta F_\nu(\hat{\gamma}_l) = \int_{4\pi} d\Omega R_s(|\hat{\gamma} - \hat{\gamma}_l|, \sigma_B) \Delta I_\nu(\hat{\gamma}) \,, \tag{17}$$

where R_s is the angular response of the receiver, say with a Gaussian beam of dispersion σ_B, whose axis coincides with the los to the cluster center. The angular dependence of ΔI_ν is fully contained in the cluster profile, and so ΔF_ν can be computed by convolving this profile with the response of the receiver. From Equations (17) and (19) the beam convolved cluster signal is:

$$\Delta F_\nu = \frac{2(kT_{CMB})^3}{(hc)^2} g(x) y_o(M, z) \Xi(M, z) \,, \tag{18}$$

where

$$\Xi \equiv \int d\Omega R_s(|\hat{\gamma} - \hat{\gamma}_l|) \zeta(|\hat{\gamma}_l|, M, z) \,. \tag{19}$$

The receiver measures the flux integrated over its passband $E(\nu)$:

$$\overline{\Delta F_\nu} = \frac{\int d\nu \Delta F_\nu E(\nu)}{\int d\nu E(\nu)} \,, \tag{20}$$

where $E(\nu)$ is the frequency response of the instrument. Thus, the predicted number of clusters with a net flux $> \overline{\Delta F_\nu}$ is

$$N(> \overline{\Delta F_\nu}) = \int \frac{dV}{dz} dz \int_{\overline{M}(\overline{\Delta F_\nu}, z)} dM N(M, z) \,, \tag{21}$$

The lower bound of the mass integral, $\overline{M}$, is determined from the requirement that the source flux is $> \overline{\Delta F_\nu}$. Equation (20) provides the mass dependence of the flux, $\Delta F_\nu(M)$, a monotonic function of the mass at a given z.

In our specific estimates of the predicted number counts for the C/S experiment, we take the spectral response to be uniform over the two passbands centered on 140 and 400 GHz with

widths $\Delta\nu/\nu = \Delta x/x = 0.4$ and 0.7, respectively. In Figures 3 and 4 we show the cluster number counts at the C/S's 140 and 400 GHz bands in the different models, with and without IC gas evolution. In Figure 5 we compare the counts expected in few models for the 400 GHz channel.

The receivers of the C/S HFI and BOOMERANG are bolometers with a Noise Equivalent Power (NEP) of $\approx 10^{-17}\ WHz^{-1/2}$. The limiting flux is expected to be

$$\overline{F}_{\nu}^{noise} \approx \frac{NEP}{\Delta\nu\sqrt{t}}\frac{1}{A\epsilon}\,, \tag{22}$$

where t is the integration time in seconds, A is the effective mirror area in squared meters, and ϵ is the total (optical and electric) efficiency of the system. For C/S, NEP values of 1.0×10^{-16} and $2.7\times10^{-17}\ WHz^{-1/2}$ are expected at 140 and 400 GHz, respectively. The C/S telescope has an effective diameter of 1 meter, and total efficiency of ≈ 0.30, so that with an integration time of one year (assuming full sky coverage) we have $\overline{F}_{\nu}^{noise} \approx 160$ and 20 mJy at 140 and 400 GHz, respectively. A similar calculation of the BOOMERANG limiting flux – with the same values of A and ϵ but with $NEP \approx 2\cdot10^{-17}$ W Hz$^{-1/2}$ and $t \approx 225$ s per pixel – yields $\overline{F}_{\nu}^{noise} \approx 20$ mJy. In Tables 3 and 4 we give the number of clusters with flux greater than $\overline{F}_{\nu}^{noise}$ and $3\overline{F}_{\nu}^{noise}$, corresponding to 1 and 3 sigma detection, respectively, as expected in the various models. Note that these numbers are obtained by requiring that the flux collected by the receiver from the center of the cluster is greater than the limiting flux. This estimate could be conservative for extended clusters if the flux emanating from the central region is under the detection limit. However, a further smoothing of the observed map could help in extracting additional clusters out of the noise (the noise of the smoothed map is lower by the factor $\theta_{smooth}/\theta_{obs}$, where θ_{smooth} and θ_{obs} are the resolutions of the smoothed and observed maps, respectively). This is reflected in Figures 3 and 4, where we show the cluster number counts expected after smoothing the original map. The noise level of the smoothed maps at 400 GHz is 10.3, 3 and 1.5 mJy for final resolutions of 10, 30 and 60 arc-minutes, respectively. Correspondingly, the number of clusters

that can be detected increases.

Even under the more conservative assumption of having just the central pixel above the limiting flux, the predicted counts are fairly large for C/S for which a full sky coverage is assumed; the quoted numbers for the BOOMERANG's 150 GHz band ($\Delta x/x = 0.2$) refer to a $10^o \times 10^o$ patch of the sky. Thus, given that the S-Z effect can be identified by virtue of its characteristic spectral signature, these experiments can, in principle, produce S-Z catalogs of clusters. Correlation analyses of S-Z and X-ray measurements of clusters will provide useful information on cluster evolution, and possibly also on cosmological scenarios.

In Figure 6 we show the redshift distribution of the predicted number of clusters seen above the limiting flux at 400 and 140 GHz. For flat (CDM and MDM) models 99% of the predicted clusters have redshifts less than $z \sim 0.2$, quite independently of the degree of gas evolution. In low density (either open or with cosmological constant) models clusters are expected also at higher redshifts ($z \lesssim 1$). However, considering gas evolution in these low density models, $\approx 90\%$ of the predicted clusters have $z \lesssim 0.3$.

Most of the detected clusters are expected to be contained just in one pixel of the mm and sub-mm maps, and so it will be difficult to clearly identify clusters under these circumstances. It is therefore important to determine also the distribution of angular sizes of clusters whose fluxes are higher than the above limiting values. This is accomplished by calculating the distribution

$$N(\theta_{FWHM}, z) = N(M, z)\frac{dM}{d\theta_c}\frac{d\theta_c}{d\theta_{FWHM}} \tag{23}$$

where $\theta_c = D_A r_c$ is the angle subtended by the core radius of a cluster, which depends on M through Equation (8), D_A is the angular diameter distance, and $\theta_{FWHM} = \theta_{FWHM}(\theta_c)$ is the FWHM of the beam convolved cluster profile:

$$\tilde{\zeta}(\theta, \sigma_B) = \frac{1}{\sigma_B^2}\int d\psi\psi\zeta(\psi)exp\Big(-\frac{\psi^2+\theta^2}{2\sigma_B^2}\Big)I_0\Big(\frac{\psi\theta}{\sigma_B^2}\Big) \tag{24}$$

In Figure 7 we show the quantity

$$\mathcal{N}(>\theta_{FWHM}) = \int_{\theta_{FWHM}}^{\infty} d\theta'_{FWHM} \int dz N(\theta'_{FWHM}, z)\,,$$

where the double integral is performed so that the mass of a cluster with a flux $> \overline{F}_{\nu}^{noise}$ is larger than a minimum value $\overline{M}$ (see Equation 23); correspondingly, at a given z, such a cluster has a FWHM angular size larger than $\overline{\theta_{FWHM}}$.

5 Discussion.

The approach described in this paper is phenomenological, as it is based on the normalization of the predicted cluster number counts so they reproduce the locally observed distribution. We consider our normalization to the XRLF to be quite robust, in the sense that a statistically significant fit to the data is obtained over a range of X-ray luminosities from $\sim 10^{43}$ to $\gtrsim 10^{45}$ erg s^{-1}. The quality of this fit is low for MDM $\Omega_\nu = 0.3$ models with scale invariant initial conditions, unless n is increased to values $\sim 1.2 \div 1.4$ (see Lucchin *et al.* 1996 for a discussion). BDM models with n in the range $-1 \div 0$ substantially overproduce the number of clusters, so the consideration of these models here is essentially motivated by didactic purposes, as an example of pure power law spectra. Affecting a different normalization – for example, normalizing directly to the mass or temperature distributions – can, in principle, yield different results, due to the different implied shapes and amplitudes of $N(M, z)$.

A comparison of the number counts for flat and low density CDM cosmologies shows that the counts increase with decreasing Ω_0. With our normalization to the XRLF, lowering Ω_0 has the effect of lowering $N(M, z)$ (which is proportional ρ) and reducing the cutoff mass. As a result, the local abundance of clusters in a low density universe is lower than in the $\Omega_0 = 1$ case, if we assume the same values for $h, \mathcal{I}$ and $b\delta_v$. This effect is counterbalanced by lowering $b\delta_v$ and increasing h and/or $\mathcal{I}$ (see Table 5). In addition, in a low density universe $N(M, z)$ evolves less than in a flat universe (see Fig.5). We stress that our scaling laws imply that the core radius

is larger in low density a universe as compared to a flat model. With all the other parameters fixed, the net flux from the cluster is then increased. Altogether, without gas evolution, we do expect a factor ≈ 5 more clusters in a low density than in a critical CDM universe. This difference is reduced when including evolution of the IC gas which has the effect of making the population of predicted clusters a more local ($z \lesssim 0.4$) one. Note the strong dependence of the counts on the assumed value of the Hubble constant.

Among the various assumptions and simplifications made in our treatment, the uniform, spherical cluster collapse – as described in the Press & Schechter (1974) formalism – is a major one. Another major uncertainty is the nature and degree of IC gas evolution. The two limiting cases considered here – no evolution, and maximum degree of evolution which is still consistent with the EMSS distant XRLFs – are likely to span a reasonably realistic range. It should also be noted that our scaling of the gas fraction to a value of 0.1 in a rich, local cluster may be conservatively low, judging by some observational indications of a value of up to 30% (see White *et al.* 1993). These uncertainties are not expected to affect our conclusion that the sky-averaged optical depth for electron scattering in the hot IC gas is quite low in all the models considered here. Obviously, the range of predicted values of τ constitutes the minimum level of scattering of the CMB eversince the epoch of last scattering. Reionization before cluster formation may have resulted in a much higher level of scattering (Tegmark & Silk 1995).

Another simplification made in our treatment is the use of the non-relativistic expression for the S-Z effect. As we have noted already, in the exact relativistic treatment the dependence of the S-Z effect is not linear in y, and the the deviation of the intensity change from the non-relativistic value is appreciable at high frequencies and gas temperatures (Rephaeli 1995b). The major contribution to the integrated effect due to the full cluster population comes from low temperature clusters. The full relativistic calculation can be affected by means of a frequency-dependent correction factor (applied to the non-relativistic expression for the intensity change)

which can be calculated at some mean, population-weighted value of the gas temperature. Since we expect this mean to be close to the lower end of the observed range, $3 \div 15$ keV, the correction will generally be small except at very high frequencies. For example, if this mean temperature is ~ 5 keV, then the correction factor is a few percent in the Rayleigh-Jeans part of the spectrum, and $\gtrsim 20\%$ at the $200 \div 240$ and $\gtrsim 600$ GHz ranges. The exact correction factors can be calculated at each frequency and gas temperature using the expressions given in Rephaeli (1995b).

The cluster number counts in the mm and sub-mm regions are of interest for upcoming high-sensitivity CMB anisotropy experimentsCMB anisotropy experiments such as BOOMERANG and C/S. The number counts shown in Table 3 are optimistic in several ways. First, sky confusion was not taken into account; its inclusion will obviously reduce our predicted numbers in a way which will largely depend on the degree of sensitivity in modeling emission from Galactic dust and far-IR emission from other galaxies. The Galactic disk region will reduce useful sky coverage to $\approx 80\%$. The integrated emission from galaxies is not known, but in some models with strong luminosity or density evolution the predicted intensity levels (e.g., Beichman and Helou 1991, Wright *et al.* 1994) may well exceed those corresponding to Comptonization . A quantitative comparison is not warranted at this stage because of the high degree of uncertainty in these models. In the analysis of actual data it will likely be possible to separate out the S-Z component based on its unique spectral shape and its larger characteristic spatial scales. For now, we include in Table 4 the numbers of clusters with $\overline{\Delta F}_\nu > 3\overline{F}_\nu^{noise}$. From these we can predict that if sky-confusion is minimal, then a full sky map – which can be generated by C/S at 400 GHz (*i.e.* , with a resolution of $4'.5$) after one year of operation – should include as many as $\approx 10^3$ clusters detected at the 3σ statistical significance level.

Appendix

The expansion rate of a low density universe is given by the Friedmann equations:

$$\dot{R}^2 = \frac{8\pi G\rho}{3}R^2 + \left\{ \begin{array}{ll} H_0^2(1-\Omega_0)R_0; & \Lambda = 0 \\ \\ H_0^2(1-\Omega_0)R^2; & \Lambda = 1-\Omega_0 \end{array} \right\} \tag{25}$$

The second terms in the rhs of the previous expressions describe the curvature and the cosmological constant contributions.

Let us consider a spherical, homogeneous perturbation. If bound, this perturbation evolves according to the following relations:

$$\dot{R}^2 = \frac{8\pi G}{3}\tilde{\rho}R^2 + \left\{ \begin{array}{ll} -c^2; & \Lambda = 0 \\ \\ (1-\Omega_0)H_0^2R^2 - c^2; & \Lambda = 1-\Omega_0 \end{array} \right\} \tag{26}$$

Here $\tilde{\rho}$ is the perturbation overdensity and the curvature terms ($\propto c^2$) are positive. Note the repulsive effect of a non vanishing cosmological constant ($\propto 1-\Omega_0$) on the perturbation evolution.

Let us assume that at some initial time t_i the fluctuation has the same size and expansion rate of the background. By subtracting Equation (27) from Equation (28) we find the conditions

$$c^2 = \frac{8\pi G}{3}\rho_i\delta_i R_i^2 + \left\{ \begin{array}{ll} -H_0^2(1-\Omega_0)R_0^2; & \Lambda = 0 \\ \\ 0; & \Lambda = 1-\Omega_0 \end{array} \right\} \tag{27}$$

Here δ_i and R_i are the density fluctuation and proper size of the perturbation, ρ_i is the background density at t_i and R_m is the proper size of the perturbation at turnaround.

Substituting Equation (29) in Equation (28) we obtain

$$3R\dot{R}^2 = 8\pi G\tilde{\rho}R^3 - 8\pi G\rho_i\delta_i R_i^2 R + \left\{ \begin{array}{ll} 3(1-\Omega_0)H_0^2RR_0^2; & \Lambda = 0 \\ \\ 3(1-\Omega_0)H_0^2R^3; & \Lambda = 1-\Omega_0 \end{array} \right\} \tag{28}$$

Imposing the turnaround condition, $\dot{R} = 0$, one finds in both cases

$$R_m^2 = \left\{ \begin{array}{ll} \dfrac{\Omega_0}{1-\Omega_0}\delta_i \dfrac{R_0}{R_i}; & \Lambda = 0 \\ \\ \dfrac{\eta}{2+\eta}\Big[\dfrac{8\pi G\rho_i\delta_i R_i^2}{3H_0^2(1-\Omega_0)}\Big]; & \Lambda = 1-\Omega_0 \end{array} \right\} \tag{29}$$

where $\eta = 3(1-\Omega_0)H_0^2/(4\pi G\tilde{\rho}_m)$. Substituting Equation (31) in Equation (30) yields:

$$3R\dot{R}^2 = 3H_0^2(1-\Omega_0)(R_m - R) \times \left\{ \begin{array}{ll} \dfrac{2}{\eta}R_m^2; & \Lambda = 0 \\ \\ (-R^2 - R_m R + \dfrac{2}{\eta}R_m^2); & \Lambda = 1-\Omega_0 \end{array} \right\} \tag{30}$$

When integrated, the previous expressions read:

$$H_0\sqrt{1-\Omega_0}\,t = \left\{ \begin{array}{ll} \sqrt{\eta/2}\displaystyle\int_0^x dx'\Big[\frac{x'}{(1-x')}\Big]^{1/2}; & \Lambda = 0 \\ \\ \displaystyle\int_0^x dx'\Big[\frac{x'}{(1-x')(2/\eta - x' - x'^2)}\Big]^{1/2}; & \Lambda = 1-\Omega_0 \end{array} \right\} \tag{31}$$

where $x = R(t)/R_m$. Analytical integration of Equation (33) with $\Lambda = 0$ provides the standard cycloid solution.

At t_i, by definition $x_i \equiv R(t_i)/R(t_m) \ll 1$: this allows a Taylor expansion of the integrands of the rhs of the previous equations and an analytical estimate of the integrals. One gets:

$$\Big(\frac{R_m}{R_i}\Big)^{3/2} = \frac{2}{3}\sqrt{\frac{\eta}{2}}\frac{1}{H_0\sqrt{1-\Omega_0}t_i} \times \left\{ \begin{array}{ll} \Big[1 + \dfrac{3}{10}\Big(\dfrac{2}{3}\sqrt{\dfrac{\eta}{2}}\dfrac{1}{H_0\sqrt{1-\Omega_0}t_i}\Big)^{-2/3}\Big]; & \Lambda = 0 \\ \\ \Big[1 + \dfrac{3}{10}\Big(1+\dfrac{\eta}{2}\Big)\Big(\dfrac{2}{3}\sqrt{\dfrac{\eta}{2}}\dfrac{1}{H_0\sqrt{1-\Omega_0}t_i}\Big)^{-2/3}\Big]; & \Lambda = 1-\Omega_0 \end{array} \right\} \tag{32}$$

We can now write the initial overdensity of the fluctuation:

$$\tilde{\rho}_i = \tilde{\rho}_m\Big(\frac{R_m}{R_i}\Big)^3 = \frac{1}{6\pi G t_i^2} \times \left\{ \begin{array}{ll} \Big[1 + \dfrac{3}{5}\Big(\dfrac{2}{3}\sqrt{\dfrac{\eta}{2}}\dfrac{1}{H_0\sqrt{1-\Omega_0}t_i}\Big)^{-2/3}\Big]; & \Lambda = 0 \\ \\ \Big[1 + \dfrac{3}{5}\Big(1+\dfrac{\eta}{2}\Big)\Big(\dfrac{2}{3}\sqrt{\dfrac{\eta}{2}}\dfrac{1}{H_0\sqrt{1-\Omega_0}t_i}\Big)^{-2/3}\Big]; & \Lambda = 1-\Omega_0 \end{array} \right\} \tag{33}$$

As both in the open and flat case $\rho_i = 1/(6\pi G t_i^2)$, given that $\tilde{\rho}_i = \rho_i(1+\delta_i)$, one finally gets:

$$\delta_i = \frac{3}{5}\Big(\frac{3}{2}\sqrt{\frac{2}{\eta}}H_0\sqrt{1-\Omega_0}t_i\Big)^{2/3} \times \left\{ \begin{array}{ll} 1; & \Lambda = 0 \\ \Big(1+\frac{\eta}{2}\Big); & \Lambda = 1-\Omega_0 \end{array} \right\} \tag{34}$$

The previous expressions give the initial density contrast (at some arbitrary early time t_i) of a perturbation that will turnaround at a given t_m. This information is contained in the η parameter through Equation (33). Substituting $t = t_m$ in eq. (31) which implies $x = 1$, we obtain a relation between the turnaround time and η. Given the parameter η we have (from its definition) the value $\tilde{\rho}_m$ of the perturbation overdensity at the turnaround time. We assume that the perturbation eventually virializes at $t_v = 3t_m$ and in this regime reaches a final dimension $R_v = R_m/2$ in the open case, and $R_v = R_m(1-\eta/2)/(2-\eta/2)$ in the $\Lambda = 1-\Omega_0$ case (see Lahav *et al.* 1991). Having determined the virialization time, t_v, and the background density at that time, we can finally evaluate the non-linear overdensity of a virialized structure

$$\Delta_v = \frac{\tilde{\rho}_v}{\rho(t_v)}. \tag{35}$$

In an open universe we can write the following analytic expression:

$$\Delta_v = \frac{18\pi^2}{\Omega_0 H_0^2 t_v^2}\frac{1}{(1+z_v)^3}\,, \tag{36}$$

where t_v and z_v are related through standard time–redshift relations.

References

Beichman, C.A. and Helou, G. 1991, ApJ, 370, L1

Cavaliere, A., Colafrancesco, S. and Menci, N. 1993, ApJ, 415, 50

Colafrancesco, S., Mazzotta, P., Rephaeli, Y. and Vittorio, N. 1994, ApJ, 433, 454

Colafrancesco, S. and Vittorio, N. 1994, ApJ, 422, 443

Cole, S. and Kaiser, N. 1988, MNRAS, 233, 637

David, L.P., Arnaud, K.A., Forman, W., & Jones, C. 1990, ApJ, 356, 32

Fixsen, D.J. *et al.* 1996, preprint

Gioia, I.M., Henry, J.P., Maccacaro, T., Morris, S.L., Stocke, J.T., & Wolter, A. 1990, ApJ, 356, L35

Henry, J.P., Gioia, I.M., Maccacaro, T., Morris, S.L., Stocke, J.T., & Wolter, A. 1992, ApJ, 386, 408

Holtzmann, J. 1989, ApJS, 71, 1

Holzapfel, W.L. *et al.* 1996, ApJ, in press

Jones, C. & Forman, W. 1992, in *Clusters and Superclusters of Galaxies*, A.C. Fabian *et al.* eds., (Cambridge: Cambridge University Press), p.

Kowalski, M.P., Ulmer, M.P., Cruddace, R.G., & Wood, K.S. 1984, ApJS, 56, 403

Lahav, O., Lilje, P.B., Primack, J.R., and Rees, M.J. 1991, MNRAS, 251, 128

Lange, A. *et al.* 1995, in "Infrared and sub-mm Space Missions in the Coming Decade", Space

Science Review, Kluwer Acad. Pub.

Lucchin, F., Colafrancesco, S., deGasperis, G., Matarrese, S., Mei, S., Mollerach, S., Moscardini, L., and Vittorio, N. 1995, ApJ, in press.

Mandolesi, R. *et al.* 1995, Planet. Space Sci., in press.

Mather, J.C., Cheng, E.S., Cottingham, D.A., Eplee, R.E., Fixsen, D.J. *et al.* 1994, ApJ, 420, 439

Press, W.H. and Schechter, P. 1974, ApJ, 187, 425

Rephaeli, Y. 1995a, ARA&A 33, 541

Rephaeli, Y. 1995b, ApJ, 445, 33

Sarazin, C.L. 1988. *X-Ray Emission from Clusters of Galaxies*, Cambridge: Cambridge University Press

Sunyaev, R.A. and Zel'dovich, Y.B. 1970, Astrophys. Sp. Sci., 7, 3

Tegmark, M., & Silk J. 1995, ApJ, 441, 458

White, S.D.M., Navarro, J.F., Evrard, A., and Frenk, C.S. 1993, Nature, 366, 429

Wright, E.L., Mather, J.C., Fixsen, D.J., Kogut, A., Shafer, R.A. *et al.* 1994, ApJ, 420, 450

Figure captions

Figure 1. The dependence of $\overline{y}$ from the maximum redshift, z_{max}, of integration [cf. Equation (16)]. A minimum mass cutoff $M_{min} = 10^{12.5}\,\mathrm{h}^{-1}\,\mathrm{M}_{\odot}$ has been chosen, corresponding to the smallest systems we consider here. Continuous and dotted curves refer to cases with and without IC gas evolution.

Figure 2. The integration domain of $N(> \overline{\Delta F}_{\nu})$ is shown for the case of a standard CDM model ($\Omega_0 = 1$, $h = 0.5$, $n = 1$) and for two different channels of the C/S experiment. The dotted contours in the Log$M$-Log$z$ plane represent isocontours of the quantity $N(M, z)\cdot M\cdot z$ and are spaced by a factor of 10, the outer contour corresponding to unity. The region contributing to the source counts is to the right of the lines $\overline{\Delta F}_{\nu} = 161$ and 19.7 mJy for the C/S's 140 and 400 Ghz channels, respectively. Heavy continuous and dashed lines refer to the cases with and without IC gas evolution.

Figure 3. Cluster number counts for the C/S 400 GHz channel for different angular resolutions (4.5 arcmin: continuos lines; 10 arcmin: dotted lines; 30 arcmin: short-dashed lines; 60 arcmin: long-dashed lines) in different models with (Figure 3a) and without (Figure 3b) IC gas evolution.

Figure 4. Same as if Figure 3 but for the C/S 140 GHz channel. In this figure we do not plot the predictions for the 4.5 arcmin resolution.

Figure 5. Comparison of the cluster number counts predicted in different models of structure formation (MDM: continuous line; open CDM: dotted line; low density, vacuum dominated CDM: short-dashed lines; standard CDM: long-dashed lines) for the C/S 400 GHz channel with (panel a) and without (panel b) IC gas evolution.

Figure 6. The redshift distribution $N(>z)$ of the cluster number counts in different models (MDM: continuous line; open CDM: dotted line; low density, vacuum dominated CDM: short-dashed lines; standard CDM: long-dashed lines) for different sensitivities: $\overline{\Delta F}_\nu = 10$ and 20 mJy (Figure 6a) and $\overline{\Delta F}_\nu = 30$ and 60 mJy (Figure 6b) for the C/S 400 GHz ($\sigma_{FWHM} = 4.5$ arcmin) and 140 GHz ($\sigma_{FWHM} = 10$ arcmin) channels. In each figure panel a) and b) refer to predictions without IC gas evolution.

Figure 7. The distribution $\mathcal{N}(>\theta_{FWHM})$ of the typical angular dimensions of the clusters above the limiting flux for the C/S 400 (Figure 7a) and 140 (Figure 7b) GHz channels. Thin lines, with (continuous) and without (dotted) IC gas evolution, refer to the distribution of intrinsic dimension. Thick lines, with (continuous) and without (dotted) IC gas evolution, refer to 4.5 and 10 arcmin smoothing of the C/S maps.

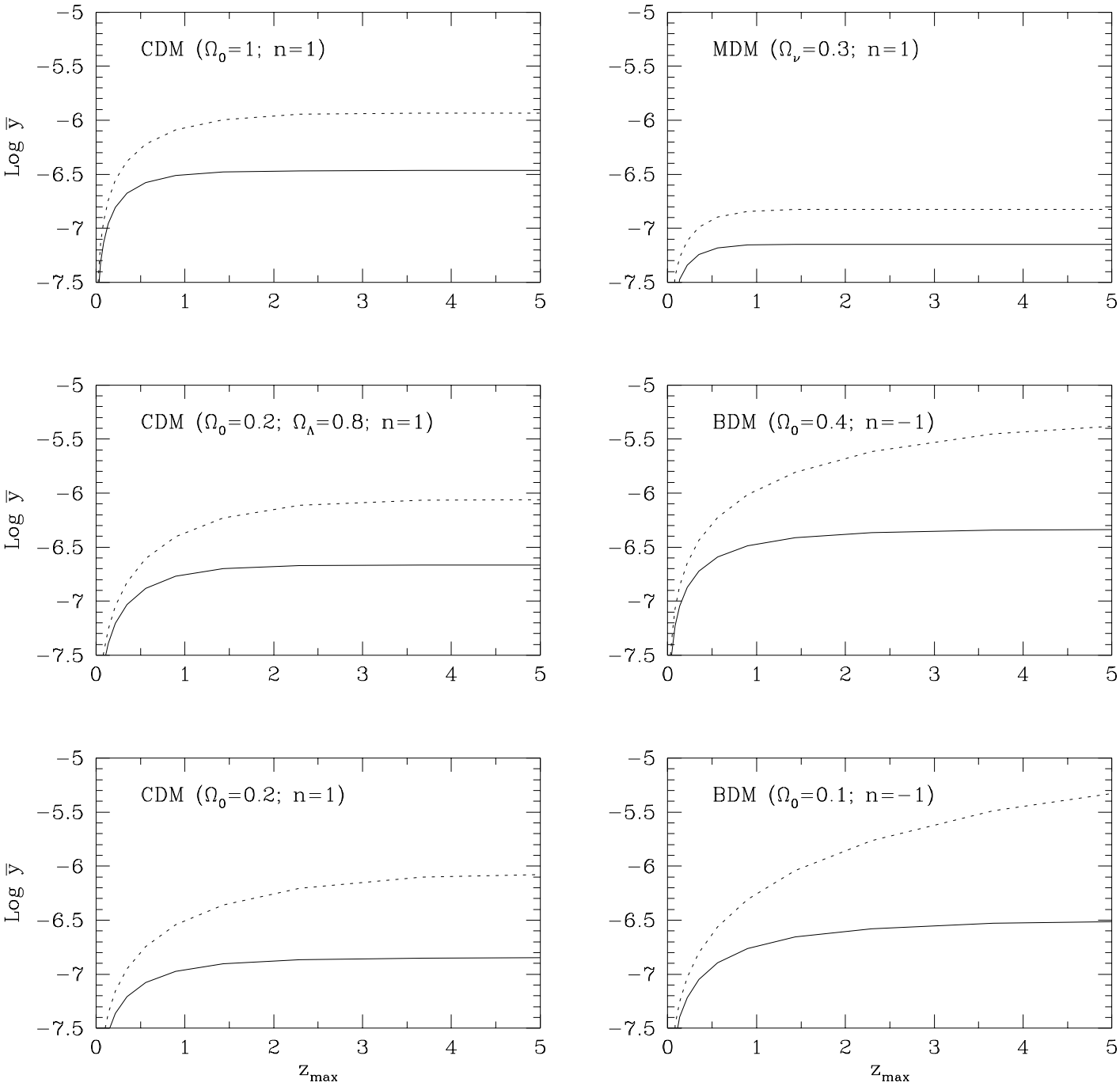
CDM (Ω_0=1; n=1)
MDM (Ω_ν=0.3; n=1)
CDM (Ω_0=0.2; Ω_Λ=0.8; n=1)
BDM (Ω_0=0.4; n=−1)
CDM (Ω_0=0.2; n=1)
BDM (Ω_0=0.1; n=−1)
Log $\bar{y}$
z_{max}
−5
−5.5
−6
−6.5
−7
−7.5
0
1
2
3
4
5

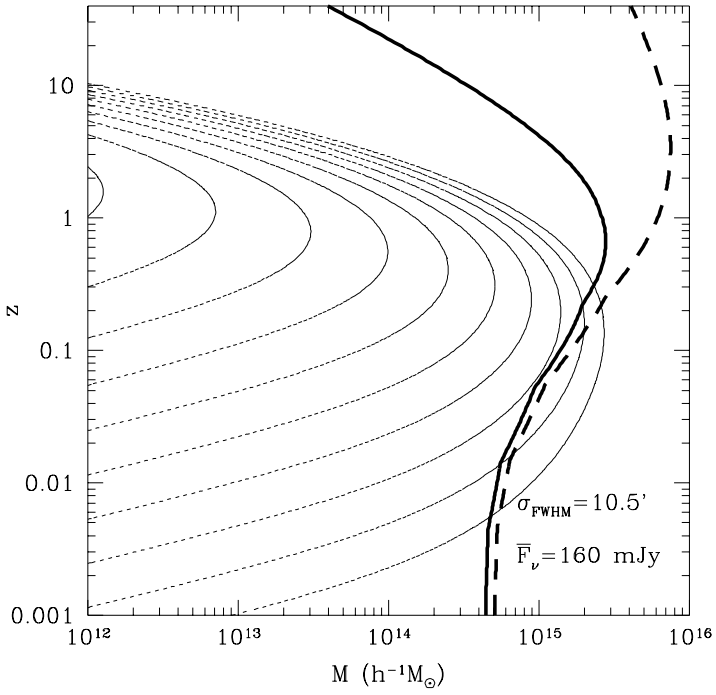
10
1
0.1
0.01
0.001
z
10^{12}
10^{13}
10^{14}
10^{15}
10^{16}
M ($h^{-1}M_{\odot}$)
σ_{FWHM}=10.5'
$\overline{F}_{\nu}$=160 mJy

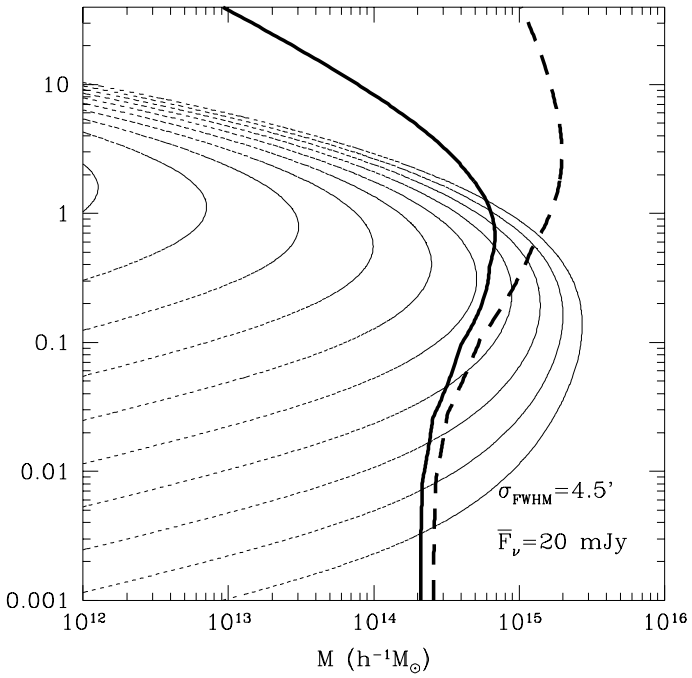
10
1
0.1
0.01
0.001
10^{12}
10^{13}
10^{14}
10^{15}
10^{16}
M ($h^{-1}M_{\odot}$)
σ_{FWHM}=4.5'
$\overline{F}_{\nu}$=20 mJy

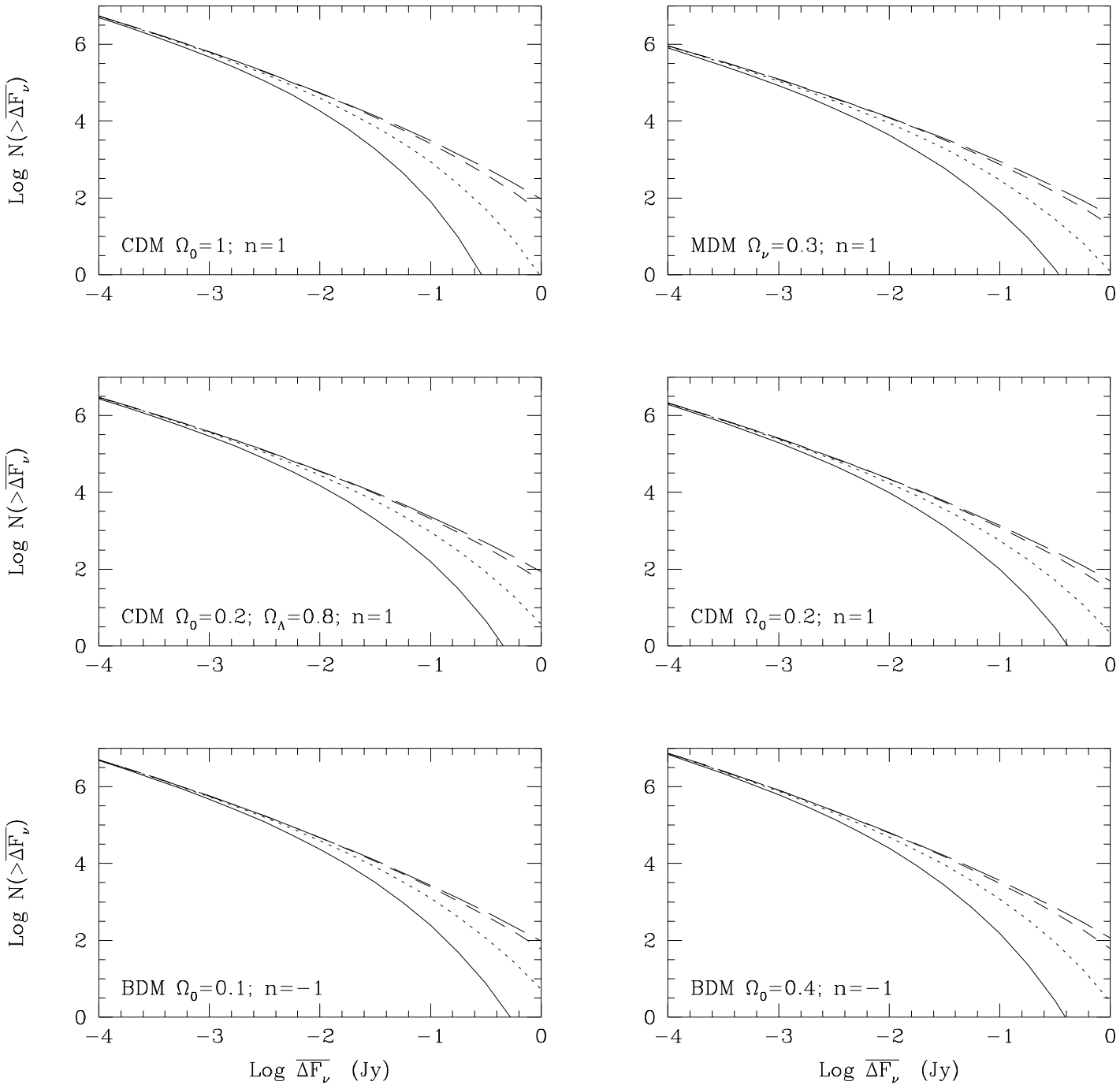
Log N(>$\overline{\Delta F_\nu}$)
CDM Ω_0=1; n=1
MDM Ω_ν=0.3; n=1
CDM Ω_0=0.2; Ω_Λ=0.8; n=1
CDM Ω_0=0.2; n=1
BDM Ω_0=0.1; n=−1
BDM Ω_0=0.4; n=−1
Log $\overline{\Delta F_\nu}$ (Jy)

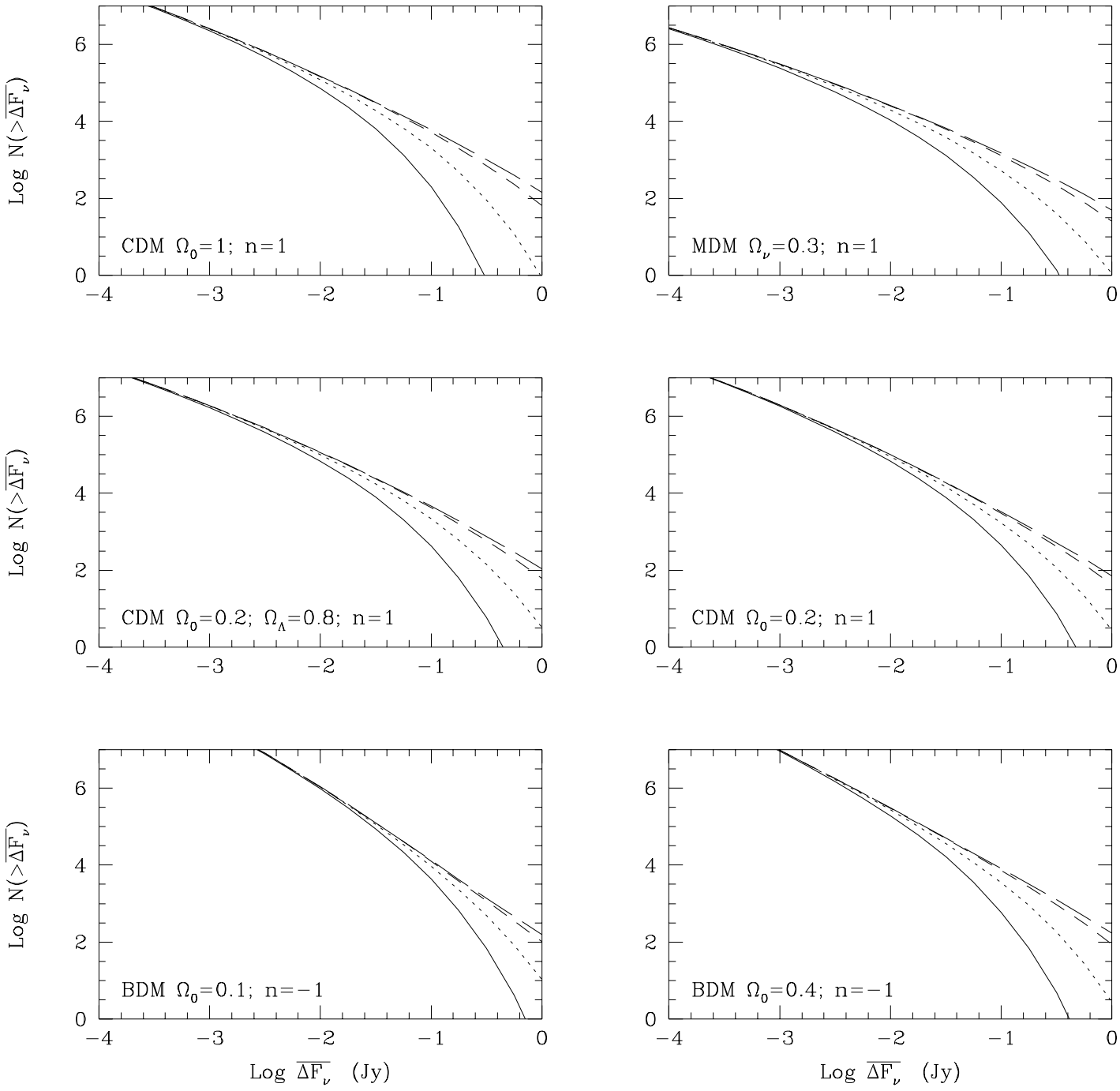
Log N(>$\overline{\Delta F_\nu}$)
CDM Ω_0=1; n=1
MDM Ω_ν=0.3; n=1
CDM Ω_0=0.2; Ω_Λ=0.8; n=1
CDM Ω_0=0.2; n=1
BDM Ω_0=0.1; n=−1
BDM Ω_0=0.4; n=−1
Log $\overline{\Delta F_\nu}$ (Jy)

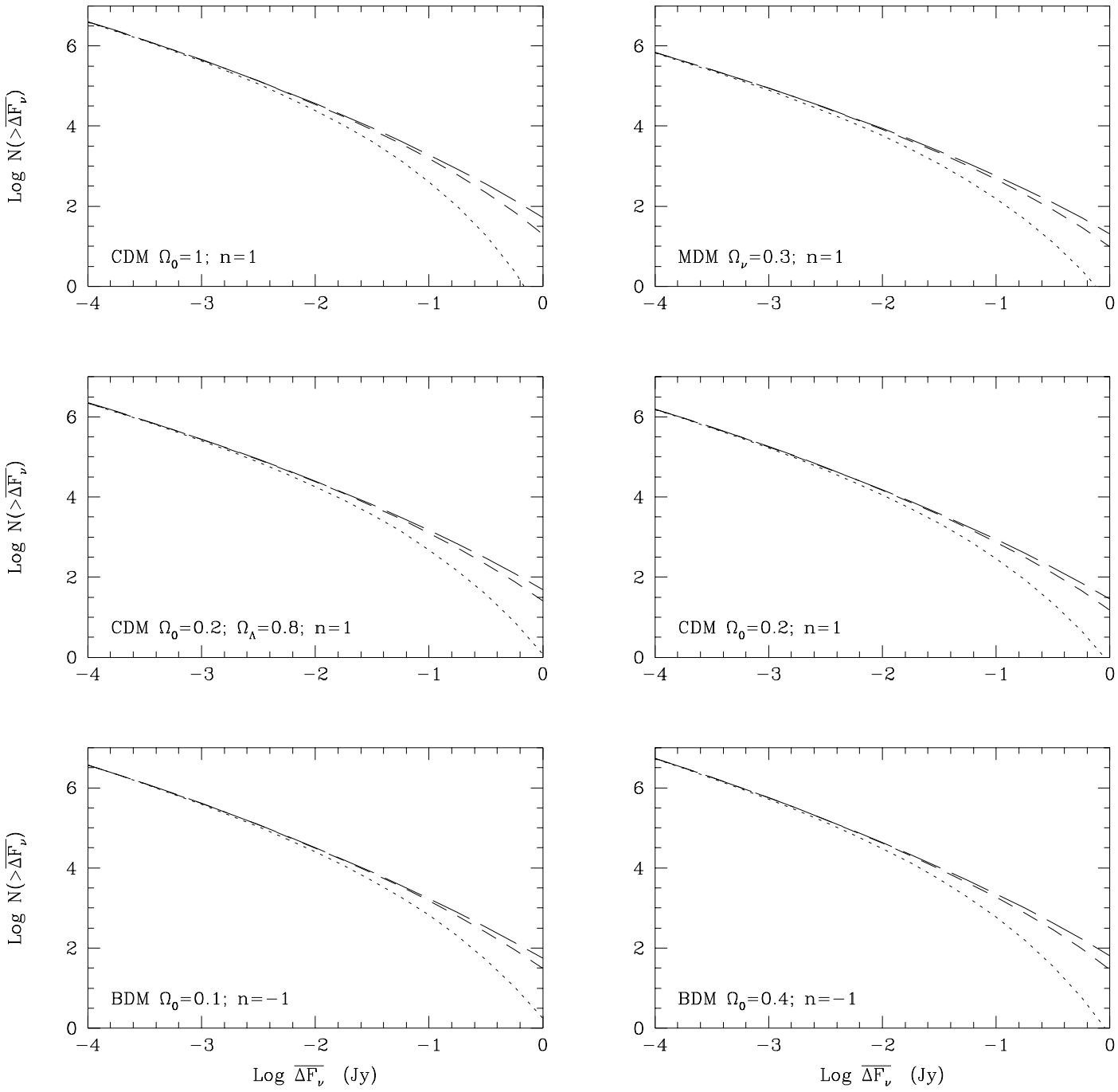
CDM Ω_0=1; n=1
MDM Ω_ν=0.3; n=1
CDM Ω_0=0.2; Ω_Λ=0.8; n=1
CDM Ω_0=0.2; n=1
BDM Ω_0=0.1; n=−1
BDM Ω_0=0.4; n=−1
Log N(>$\overline{\Delta F_\nu}$)
Log $\overline{\Delta F_\nu}$ (Jy)
0
2
4
6
−4
−3
−2
−1
0

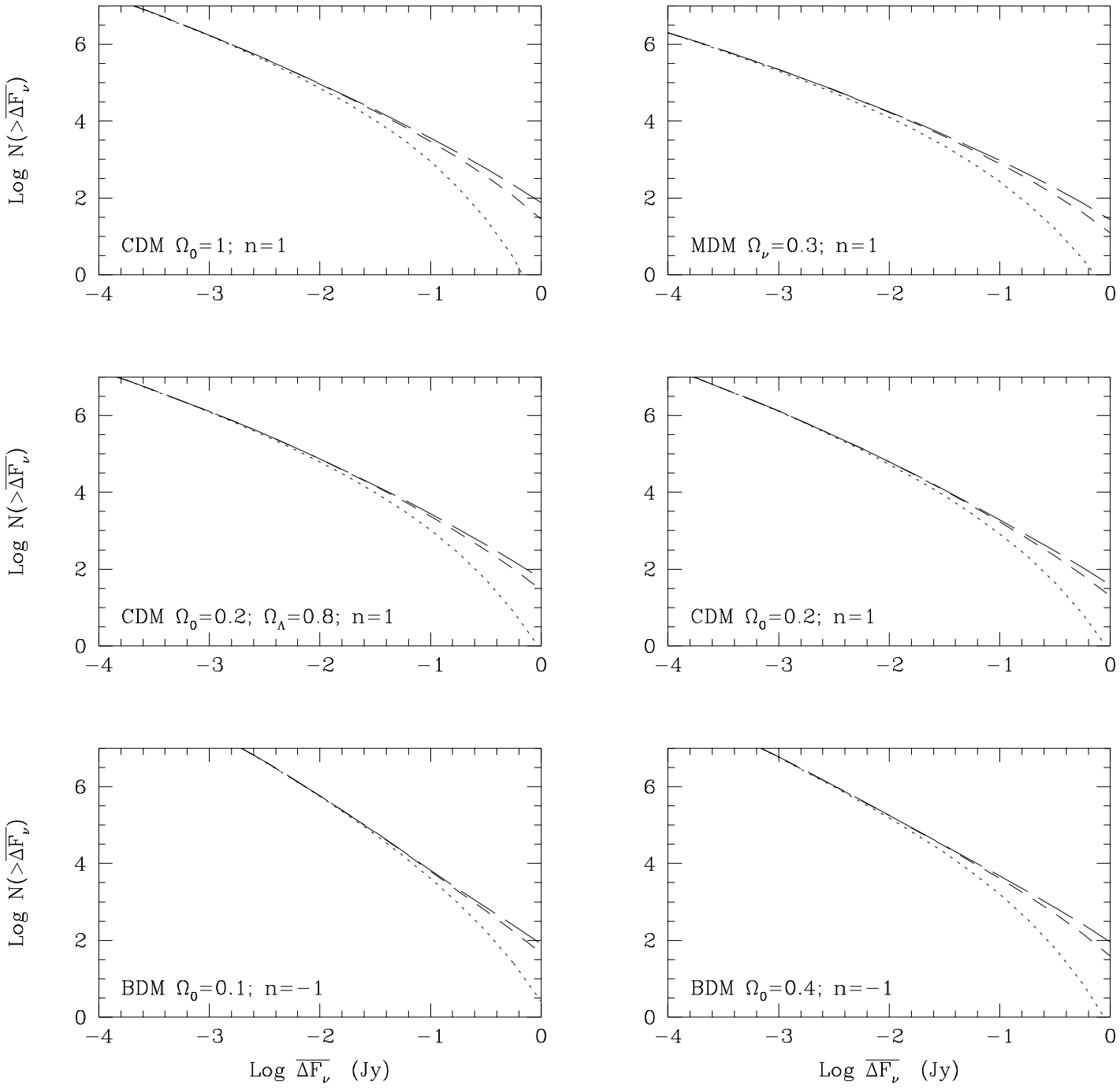
Log N(>$\overline{\Delta F_\nu}$)
CDM Ω_0=1; n=1
MDM Ω_ν=0.3; n=1
CDM Ω_0=0.2; Ω_Λ=0.8; n=1
CDM Ω_0=0.2; n=1
BDM Ω_0=0.1; n=−1
BDM Ω_0=0.4; n=−1
Log $\overline{\Delta F_\nu}$ (Jy)

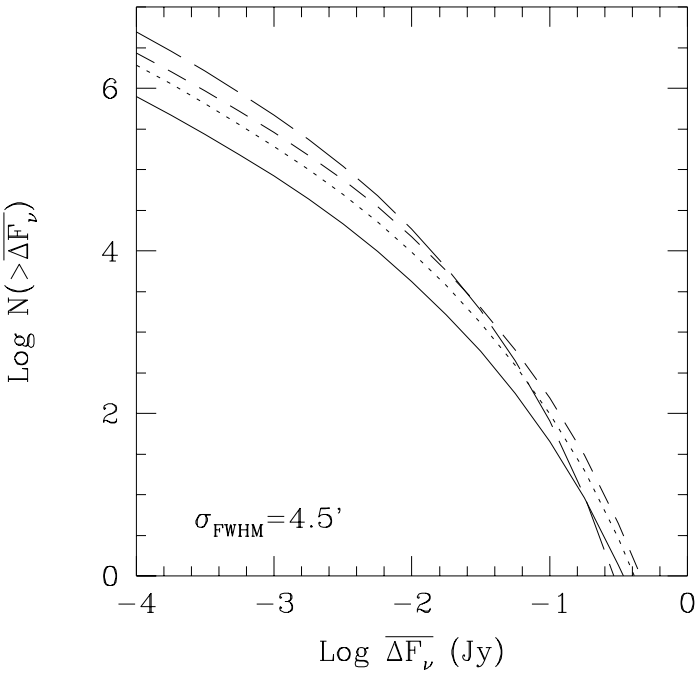
Log N(>$\overline{\Delta F_\nu}$)
6
4
2
0
−4
−3
−2
−1
0
σ_{FWHM}=4.5'
Log $\overline{\Delta F_\nu}$ (Jy)

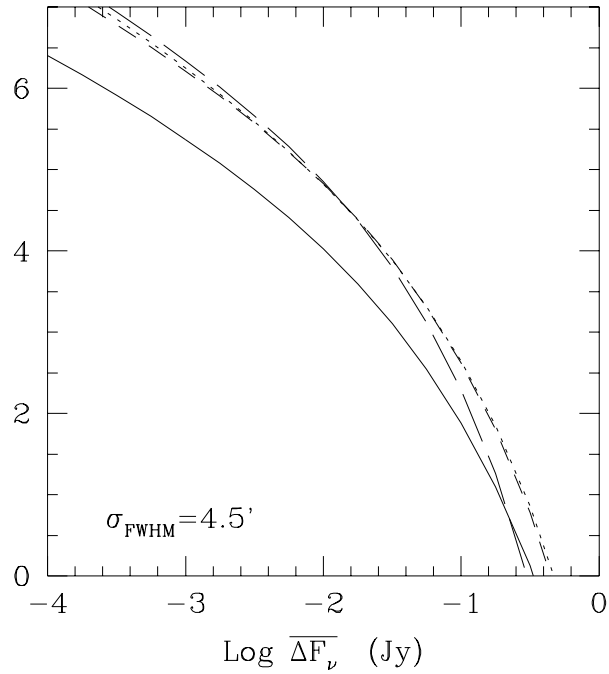
6
4
2
0
−4
−3
−2
−1
0
σ_{FWHM}=4.5'
Log $\overline{\Delta F_\nu}$ (Jy)

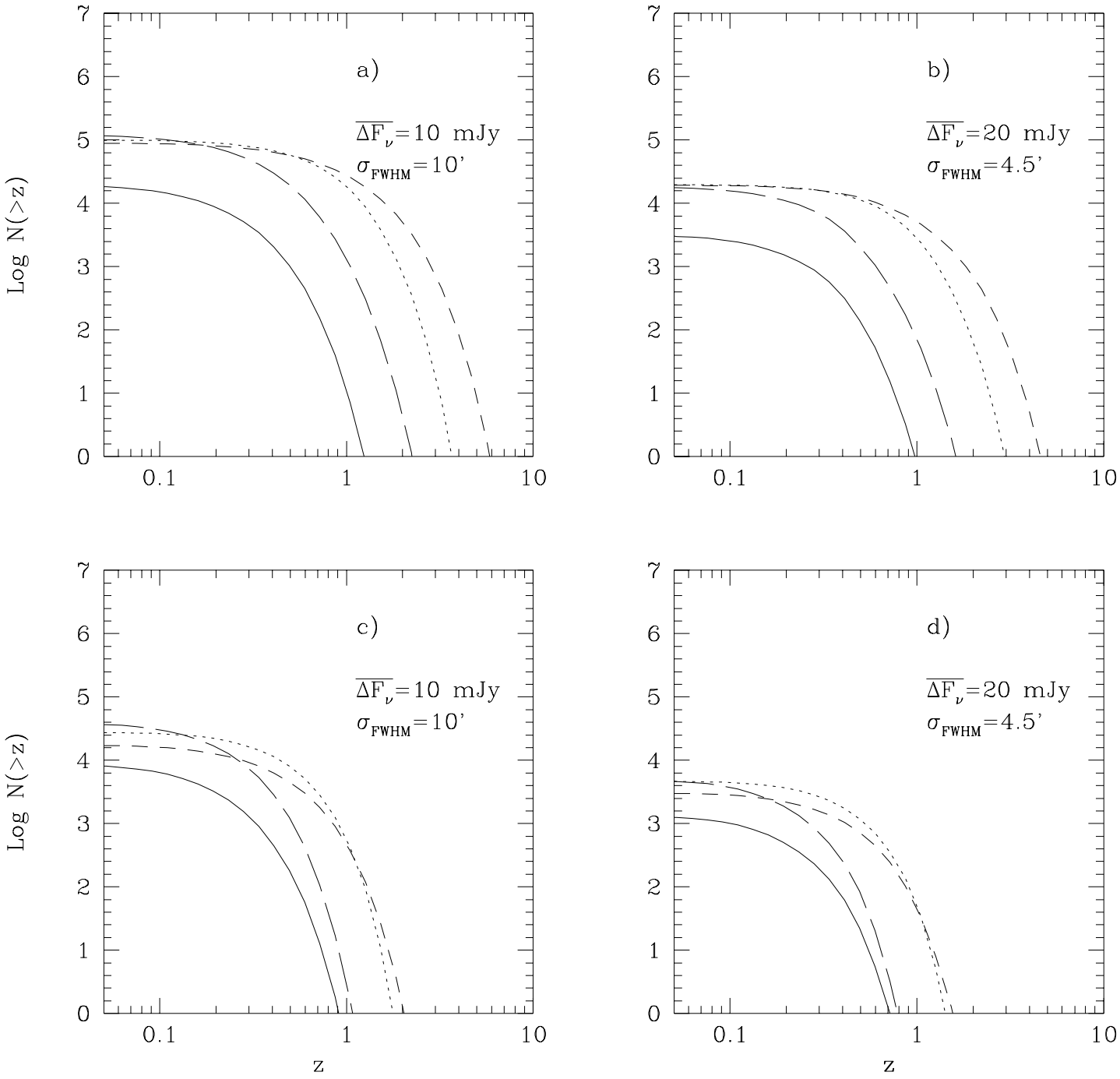
a)
$\overline{\Delta F_\nu}$=10 mJy
σ_{FWHM}=10'
b)
$\overline{\Delta F_\nu}$=20 mJy
σ_{FWHM}=4.5'
c)
$\overline{\Delta F_\nu}$=10 mJy
σ_{FWHM}=10'
d)
$\overline{\Delta F_\nu}$=20 mJy
σ_{FWHM}=4.5'
Log N(>z)
z
0
1
2
3
4
5
6
7
0.1
1
10

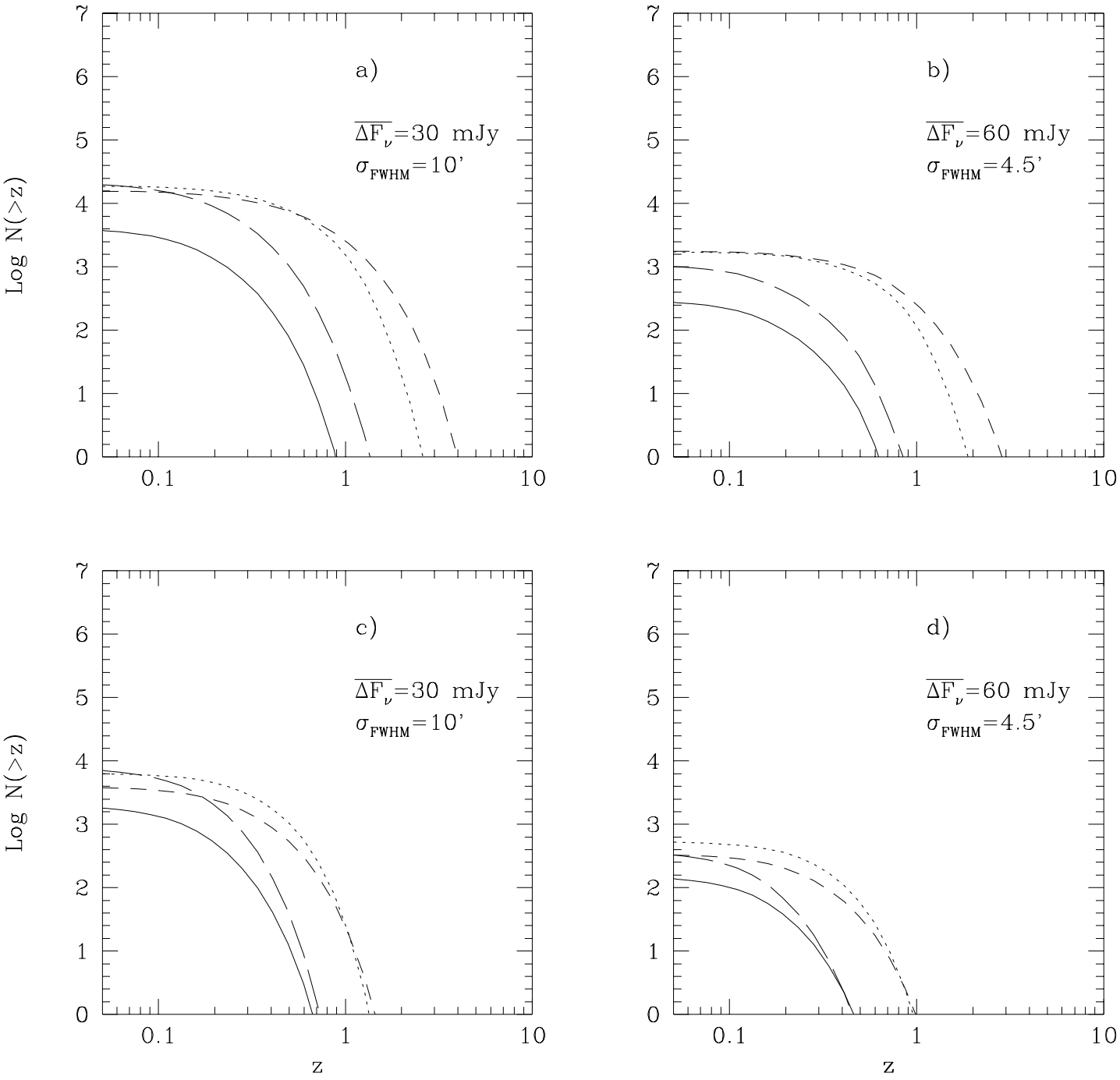
a)
$\overline{\Delta F_\nu}$=30 mJy
σ_{FWHM}=10'
b)
$\overline{\Delta F_\nu}$=60 mJy
σ_{FWHM}=4.5'
c)
$\overline{\Delta F_\nu}$=30 mJy
σ_{FWHM}=10'
d)
$\overline{\Delta F_\nu}$=60 mJy
σ_{FWHM}=4.5'
Log N(>z)
z
0
1
2
3
4
5
6
7
0.1
1
10

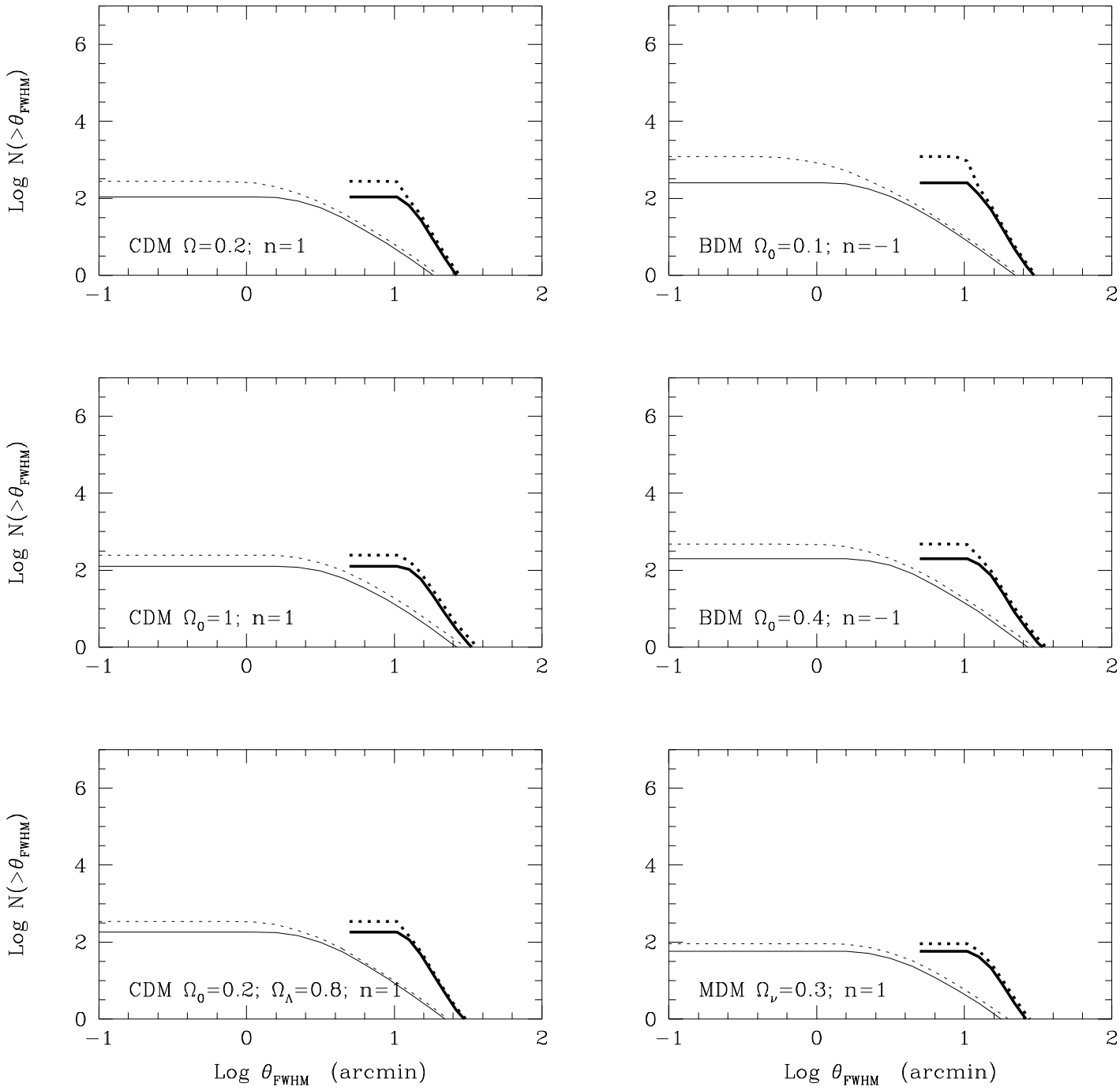
Log N(>θ_FWHM)
CDM Ω=0.2; n=1
BDM Ω_0=0.1; n=−1
CDM Ω_0=1; n=1
BDM Ω_0=0.4; n=−1
CDM Ω_0=0.2; Ω_Λ=0.8; n=1
MDM Ω_ν=0.3; n=1
Log θ_FWHM (arcmin)

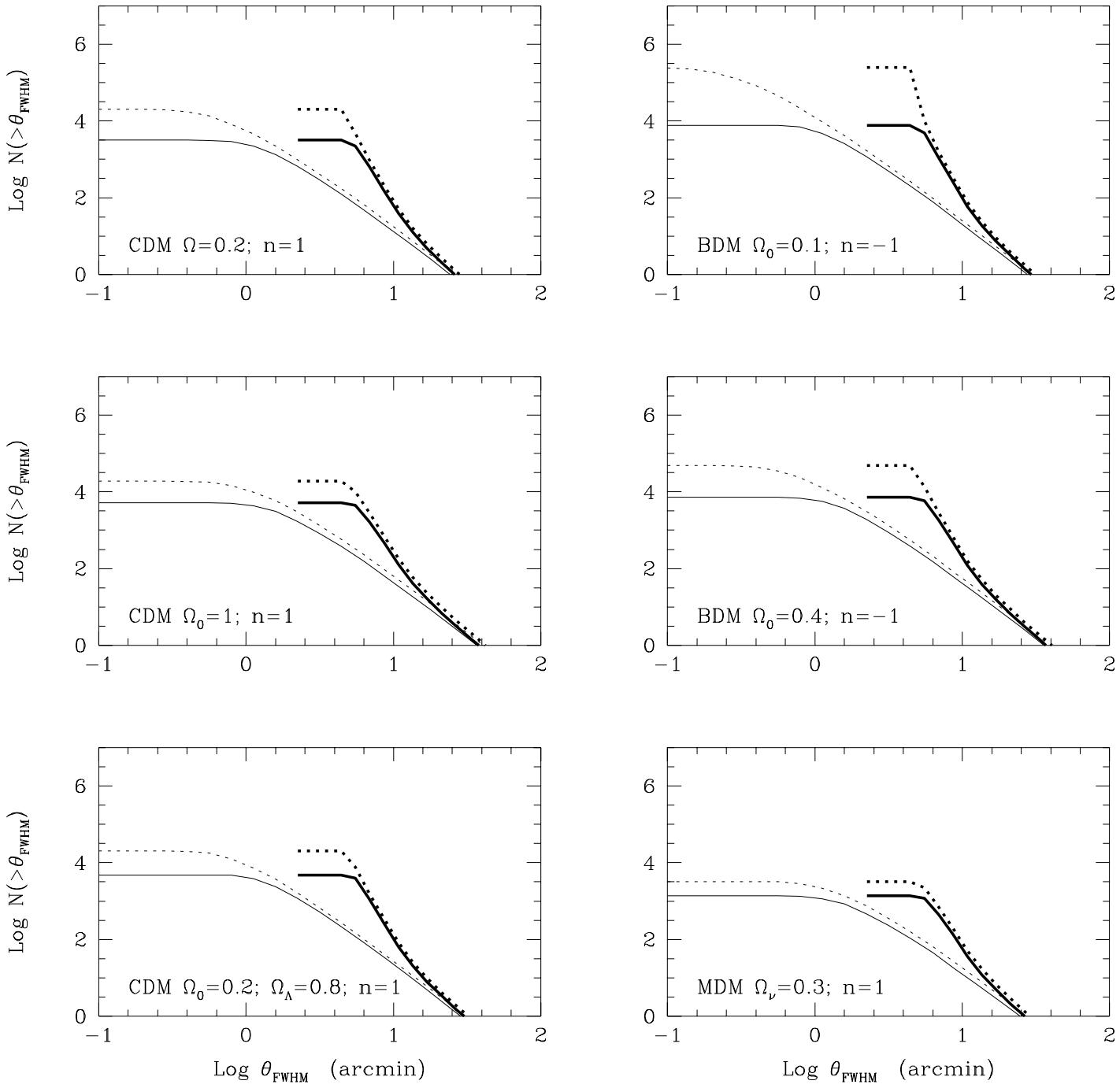
Log N(>θ_FWHM)
CDM Ω=0.2; n=1
BDM Ω_0=0.1; n=−1
CDM Ω_0=1; n=1
BDM Ω_0=0.4; n=−1
CDM Ω_0=0.2; Ω_Λ=0.8; n=1
MDM Ω_ν=0.3; n=1
Log θ_FWHM (arcmin)

Table 2

Models	<y> in units of 10^{-6}					
	with ICM evolution			without ICM evolution		
	$10^{13}M_o$	$10^{13.5}M_o$	$10^{14}M_o$	$10^{13}M_o$	$10^{13.5}M_o$	$10^{14}M_o$
CDM						
Ω=1.0; h=0.5						
n=1	0.34	0.30	0.23	1.17	0.86	0.52
n=0.8	0.30	0.27	0.21	0.92	0.71	0.45
CDM+Λ						
Ω=0.2; n=1						
h=0.5	0.27	0.26	0.23	0.99	0.82	0.61
h=0.6	0.22	0.20	0.17	0.88	0.70	0.48
h=0.7	0.18	0.16	0.13	0.77	0.58	0.37
CDM open						
Ω=0.2;n=1						
h=0.5	0.20	0.18	0.16	1.16	0.89	0.60
h=0.6	0.14	0.13	0.11	0.88	0.63	0.38
h=0.7	0.12	0.11	0.08	0.77	0.52	0.28
MDM						
Ω_ν=0.3;h=0.5						
n=1.0	0.07	0.06	0.05	0.15	0.12	0.08
n=1.2	0.10	0.09	0.07	0.24	0.19	0.12
n=1.4	0.16	0.14	0.11	0.41	0.31	0.20
BDM						
Ω=0.1; n=-1						
h=0.5	0.43	0.41	0.37	27.3	15.0	7.25
h=0.6	0.33	0.31	0.27	18.9	9.76	4.27
h=0.7	0.25	0.23	0.19	13.2	6.41	2.54
BDM						
Ω=0.4; n=-1						
h=0.5	0.46	0.42	0.34	5.19	3.04	1.53
h=0.6	0.35	0.31	0.23	3.79	2.08	0.94
h=0.7	0.32	0.27	0.19	3.38	1.78	0.74

Table 3

Models	$\langle\tau\rangle$ in units of 10^{-4}					
	with ICM evolution			without ICM evolution		
	$10^{13}M_o$	$10^{13.5}$ M_o	$10^{14}M_o$	$10^{13}M_o$	$10^{13.5}$ M_o	$10^{14}M_o$
CDM						
Ω=1.0; h=0.5						
n=1	1.53	1.04	0.56	6.58	3.34	1.34
n=0.8	1.27	0.88	0.49	5.05	2.68	1.14
CDM+Λ						
Ω=0.2; n=1						
h=0.5	0.84	0.65	0.45	4.75	2.74	1.38
h=0.6	0.79	0.59	0.37	4.56	2.47	1.13
h=0.7	0.75	0.53	0.30	4.28	2.18	0.90
CDM open						
Ω=0.2;n=1						
h=0.5	0.57	0.43	0.29	4.72	2.50	1.14
h=0.6	0.50	0.36	0.21	4.01	1.96	0.79
h=0.7	0.48	0.32	0.17	3.70	1.69	0.61
MDM						
Ω_ν=0.3;h=0.5						
n=1.0	0.34	0.22	0.12	0.91	0.50	0.22
n=1.2	0.50	0.33	0.17	1.49	0.78	0.33
n=1.4	0.76	0.50	0.26	2.51	1.29	0.53
BDM						
Ω=0.1; n=-1						
h=0.5	0.81	0.69	0.51	58.3	23.8	8.42
h=0.6	0.77	0.62	0.43	45.1	17.2	5.55
h=0.7	0.69	0.53	0.33	35.0	12.5	3.63
BDM						
Ω=0.4; n=-1						
h=0.5	1.63	1.21	0.73	22.2	9.31	3.28
h=0.6	1.45	1.01	0.54	17.8	6.93	2.15
h=0.7	1.38	0.92	0.45	16.2	5.98	1.69

Table 4

Models	$N(>F_\nu^{noise})$					
	with ICM evolution			without ICM evolution		
	4.5′ 400GHz	5′ 150GHz	10.5′ 140GHz	4.5′ 400GHz	5′ 150GHz	10.5′ 140GHz
CDM						
Ω=1.0; h=0.5						
n=1	4981	7	146	18258	25	286
n=0.8	5206	8	181	18034	25	347
CDM+Λ						
Ω=0.2; n=1						
h=0.5	7094	11	350	26336	38	611
h=0.6	4698	7	200	19722	28	376
h=0.7	3194	5	118	14583	20	233
CDM open						
Ω=0.2;n=1						
h=0.5	5518	9	260	32821	47	631
h=0.6	3065	5	121	19426	27	297
h=0.7	2157	3	75	14735	20	195
MDM						
Ω_ν=0.3;h=0.5						
n=1.0	1348	2	65	3176	5	101
n=1.2	1745	3	74	4526	7	122
n=1.4	2599	4	101	7422	11	175
BDM						
Ω=0.1; n=-1						
h=0.5	12114	19	494	414779	511	2652
h=0.6	7511	7	273	237724	284	1295
h=0.7	4525	7	150	138250	161	666
BDM						
Ω=0.4; n=-1						
h=0.5	6930	10	226	26597	60	525
h=0.6	4145	6	120	29466	37	302
h=0.7	3611	5	104	27995	35	283

Table 5

Models	N (> $2F_\nu^{noise}$) at 400 GHz	
	with ICM evolution	without ICM evolution
CDM		
Ω=1.0; h=0.5		
n=1	1063	3459
n=0.8	1220	3792
CDM+Λ		
Ω=0.2; n=1		
h=0.5	2068	6828
h=0.6	1259	4648
h=0.7	786	3111
CDM open		
Ω=0.2;n=1		
h=0.5	1629	8872
h=0.6	810	4656
h=0.7	528	3261
MDM		
Ω_ν=0.3;h=0.5		
n=1.0	364	771
n=1.2	441	1027
n=1.4	633	1620
BDM		
Ω=0.1; n=-1		
h=0.5	3449	95100
h=0.6	1975	49832
h=0.7	1105	26549
BDM		
Ω=0.4; n=-1		
h=0.5	1600	9011
h=0.6	875	5205
h=0.7	750	4889

Table 1

Models	**Fit parameters**				
	h	I	$b \cdot \delta_\nu$	η	ξ
CDM Ω=1.0					
n=1	0.5	1	2.5	0.2	1.2
n=0.8	0.5	1	2.45	0.2	1.2
CDM+Λ; Ω=0.2; n=1					
	0.5	1	1.3	0.2	1.45
	0.6	1	1.4	0.2	1.6
	0.7	1	1.5	0.2	1.7
CDM; Ω=0.2; n=1					
	0.5	1	1.4	0.2	1.6
	0.6	1	1.55	0.2	1.7
	0.7	1	1.65	0.2	1.8
MDM; Ω_ν=0.3					
n=1.0	0.5	1	2.8	0.2	0.8
n=1.2	0.5	1	2.75	0.2	0.9
n=1.4	0.5	1	2.65	0.2	1.0
BDM; Ω=0.1; n=-1					
	0.5	1	0.7	0.2	2.0
	0.6	1	0.8	0.2	2.1
	0.7	1	0.9	0.2	2.25
BDM; Ω=0.4; n=-1					
	0.5	1	1.5	0.2	1.7
	0.6	1	1.7	0.2	1.85
	0.7	1	1.8	0.2	2.0